Improvement of ENSO Simulation Based on Intermodel Diversity

YOO-GEUN HAM

Faculty of Earth Systems and Environmental Sciences, Chonnam National University, Gwangju, South Korea

JONG-SEONG KUG

School of Environmental Science and Engineering, Pohang University of Science and Technology, Pohang, South Korea

(Manuscript received 27 May 2014, in final form 24 September 2014)

ABSTRACT

In this study, a new methodology is developed to improve the climate simulation of state-of-the-art coupled global climate models (GCMs), by a postprocessing based on the intermodel diversity. Based on the close connection between the interannual variability and climatological states, the distinctive relation between the intermodel diversity of the interannual variability and that of the basic state is found. Based on this relation, the simulated interannual variabilities can be improved, by correcting their climatological bias. To test this methodology, the dominant intermodel difference in precipitation responses during El Niño–Southern Oscillation (ENSO) is investigated, and its relationship with climatological state. It is found that the dominant intermodel diversity of the ENSO precipitation in phase 5 of the Coupled Model Intercomparison Project (CMIP5) is associated with the zonal shift of the positive precipitation center during El Niño. This dominant intermodel difference is significantly correlated with the basic states. The models with wetter (dryer) climatology than the climatology of the multimodel ensemble (MME) over the central Pacific tend to shift positive ENSO precipitation anomalies to the east (west). Based on the model's systematic errors in atmospheric ENSO response and bias, the models with better climatological state tend to simulate more realistic atmospheric ENSO responses.

Therefore, the statistical method to correct the ENSO response mostly improves the ENSO response. After the statistical correction, simulating quality of the MME ENSO precipitation is distinctively improved. These results provide a possibility that the present methodology can be also applied to improving climate projection and seasonal climate prediction.

1. Introduction

Since the fundamental ENSO theory was established, there has been tremendous improvement over the last three decades or so in modeling the ENSO variability, using atmosphere–ocean global climate models (AOGCMs) (Guilyardi et al. 2009). As well as the improvement of the individual model that has been reported in terms of ENSO-related atmospheric–ocean coupled feedbacks, in addition to the overall ENSO variability (Kim et al. 2008; Neale et al. 2008; Watanabe et al. 2010; Gent et al. 2011; Ham et al. 2010, 2012), a group of models that participated in the most recent phase (5) of the Coupled Model Intercomparison Project (i.e., CMIP5; Taylor et al. 2012) have the ability to simulate a more realistic ENSO than those in previous phases of CMIP (e.g., CMIP2 or CMIP3) (AchutaRao and Sperber 2006; Kug et al. 2012; Kim and Yu 2012; Kim et al. 2013; Bellenger et al. 2014).

However, there are still several systematic problems in simulating sea surface temperature (SST) variability during the ENSO, using the state-of-the-art AOGCMs. One of the common problems is that the center of the ENSO-related SST variability over the tropical Pacific shifts to the west, compared to the observed location (Kug et al. 2012; Capotondi and Wittenberg 2013), and sometimes it extends too far into the western Pacific, where there is a negative SST anomaly in the observation during El Niño (Ham et al. 2012, 2014). Those systematic differences between the simulated and the observed ENSO SST cause a relatively lower seasonal

Corresponding author address: Prof. Jong-Seong Kug, School of Environmental Science and Engineering, POSTEC, 77 Cheongam-Ro, Nam-Gu, Pohang 790-784, South Korea.
E-mail: jskug1@gmail.com

DOI: 10.1175/JCLI-D-14-00376.1

forecasting skill using the climate model over the equatorial western and far eastern Pacific than over other regions (Ham et al. 2014). It is also problematic that the meridional width of the simulated ENSO SST is not as wide as the observed width (Neale et al. 2008; Zhang and Jin 2012). In addition, most of the climate models still have difficulties in simulating two independent types of El Niño events [i.e., the central Pacific (CP) and eastern Pacific (EP) types of El Niño] (Yu and Kim 2010; Ham and Kug 2012; Kug et al. 2012; Yeh et al. 2014b; Jang et al. 2013).

Those systematic errors in the ENSO-related SST are strongly coupled with those of atmospheric variability during the ENSO event. Consistent with the westward shift of the center of the ENSO SST anomalies, the positive precipitation anomalies during El Niño are also shifted to the west (Misra et al. 2007). In addition, the extension of positive SST anomalies to the tropical western Pacific rather increases the local convective activity, where negative precipitation anomalies are observed during El Niño events (Ham and Kug 2014). Those systematic errors in the precipitation response are reported to be responsible for the failure of simulating two types of El Niño events in climate models (Ham and Kug 2012). Also, it is responsible for the westward extension of ENSO-related positive zonal wind stress anomalies (Kirtman et al. 2002), which induces the shortened period of the ENSO (Neale et al. 2008) or unrealistic ENSO phase-locking (Ham et al. 2012; Ham and Kug 2014). In addition, the narrow zonal wind stress response in the latitudinal direction also contributes to the shorter period of the ENSO in climate models. These are all crucial issues, as the quality of simulating realistic ENSO-related atmospheric responses determines the quality of the midlatitude teleconnection pattern during El Niño (Spencer and Slingo 2003).

However, those common systematic errors in the ENSO-related atmospheric response are not fully described, and are only partially reported in previous studies. That is, just what the common systematic errors in the simulated ENSO-related fields are has not yet been quantitatively investigated, nor what can be related to those systematic errors. That might be due to the fact that the systematic errors in ENSO-related variables are too diverse from model to model (Dai 2006), as they are determined by model formulations that vary considerably among climate models. These errors are also caused by various spatial distributions of the mean state (Choi et al. 2012; Yeh et al. 2012), the strength of the annual cycle (Kirtman et al. 2002; An et al. 2010), and various air–sea coupled feedbacks (Kim et al. 2013; Yeh et al. 2014a) in climate models.

The linkage between the mean bias (i.e., error in the mean state) and the systematic error in the ENSO properties is based on the notion that the ENSO properties are dependent on the tropical mean state. Fedorov and Philander (2001) argued that the excitation of two distinct unstable modes related to the ENSO is controlled by the mean thermocline depth and the strength of the mean easterly winds. ENSO with a longer period is related to a relatively deep thermocline depth, whereas ENSO with short periods is associated with shallow thermocline depth. As well as the period and amplitude of the ENSO, two distinct modes are linked to different SST action centers, implying that the climatological state can control the spatial pattern of ENSO (Bejarano and Jin 2008). Their findings are supported by the decadal modulation of ENSO properties (Wang and An 2001; An et al. 2010; Choi et al. 2011). An et al. (2010) showed that the decades with a warm mean state over the western Pacific are the periods when the amplitude of the ENSO is reduced. In addition, Choi et al. (2011) argued that decades with western Pacific warming and associated subsurface temperature change in the mean state are when the SST action center shifts to the west (i.e., higher occurrence of CP-type El Niño). They additionally emphasized that the increased climatological convection over the western Pacific related to the local SST warming also acts to move the ENSO-related convective activity and SST action center to the west.

A similar dynamical connection between the mean bias and systematic errors during the ENSO in climate models is reported in previous studies (Lau and Nath 2000; Annamalai and Liu 2005; Turner et al. 2005; Annamalai et al. 2007). Turner et al. (2005) demonstrated that the correction of systematic model error in the coupled model using ocean-surface heat flux adjustment has significant benefits in improving the monsoon–ENSO teleconnection. Ham et al. (2013) pointed out that the version of the Seoul National University (SNU) model with deeper mean thermocline depth over the equatorial central Pacific has less occurrence of CP El Niño. Jang et al. (2013) argued that the wet mean precipitation over the western Pacific is responsible for the quality of simulating two types of El Niño events, by modifying the ENSO-related atmospheric response. Ham and Kug (2014) also showed that the mean bias in the precipitation plays a role in determining the quality of ENSO phase-locking in CMIP models.

This raises an important question, in terms of both the climate modeling and understanding systematic errors: Does the model with better climatology have less systematic errors? To answer this question, it is worthwhile to investigate the intermodel difference in the systematic errors. In addition, as probably not all of

TABLE 1. Description of the model from the CMIP5 archives.

Modeling group	Model number	CMIP model	Integration period (yr)
MPI-M	1	MPI-ESM-LR	156
CSIRO/Queensland Climate Change Centre of Excellence (QCCCE)	2	CSIRO-Mk3.6.0	156
NOAA/GFDL	3	GFDL-ESM2G	156
MPI-M	4	MPI-ESM-MR	156
IPSL	5	IPSL-CM5A-LR	156
IPSL	6	IPSL-CM5A-MR	156
CCSR, JAMSTEC	7	MIROC-ESM-CHEM	156
CCSR, JAMSTEC	8	MIROC-ESM	156
Met Office Hadley Centre	9	HadGEM2-ES	146
INM	10	INM-CM4	156
CCSR, JAMSTEC	11	MIROC5	156
NOAA/GFDL	12	GFDL-CM3	156
Norwegian Climate Centre (NCC)	13	NorESM1-ME	156
NCAR	14	CESM1-CAM5	156
NASA GISS	15	GISS-E2-H-CC	156
Met Office Hadley Centre	16	HadGEM2-AO	156
NCC	17	NorESM1-M	156
College of Global Change and Earth System Science (GCESS), Beijing Normal University	18	BNU-ESM	156
NOAA/GFDL	19	GFDL-ESM2M	156
Meteorological Research Institute (MRI)	20	MRI-CGCM3	156
Met Office Hadley Centre	21	HadGEM2-CC	146
CCCma	22	CanESM2	156
Bjerknes Centre for Climate Research (BCCR)	23	BCC-CSM1.1(m)	156
CMCC	24	CMCC-CM5	156
NASA GISS	25	GISS-E2-H	156
NCAR	26	CCSM4	156
NCAR	27	CESM4-BGC	156
First Institute of Oceanography (FIO)	28	FIO-ESM	156
Météo-France	29	CNRM-CM5	156
BCCR	30	BCC-CSM1.1	156
CMCC	31	CMCC-CM	156
IPSL	32	IPSL-CM5B-LR	156
NASA GISS	33	GISS-E2-R-CC	156
NASA GISS	34	GISS-E2-R	156

the systematic errors related to the ENSO are due to the mean state, we have to raise the following question, to answer the first one: Which part of the systematic error is well linked to (or caused by) the mean state? Once it is detected, can we identify whether the systematic error related to the mean state is the dominant one?

Therefore, in this study, the dominant intermodel difference in the systematic error related to the ENSO will be detected by analyzing the multimodel output in CMIP5 and investigating those dominant error patterns that are associated with the mean state. Then, we will check whether the model with smaller mean bias suffers fewer systematic errors related to ENSO. Section 2 describes the CMIP5 and observational data used in this study. In section 3, we will show the intermodel differences in the ENSO-related atmospheric responses and link them with the differences in the climatological state. Section 4 introduces the method to improve the ENSO systematic error through the mean bias correction. A summary and conclusions are presented in section 5.

2. Model outputs and observational data

The historical integrations produced by the CMIP5 models are used in this study. Thirty-four climate models with single ensemble are analyzed. Note that the CMIP5 models are selected based on the availability at the analyzing time. Model references, details on the institutions where the models were run, and the integration periods are summarized in Table 1. Except for two models, the total integration period is 156 years from 1850, but all analyses in this study are based on the period from 1950. Note that the major results are not sensitive to the data period. The linear trend is removed before the analysis.

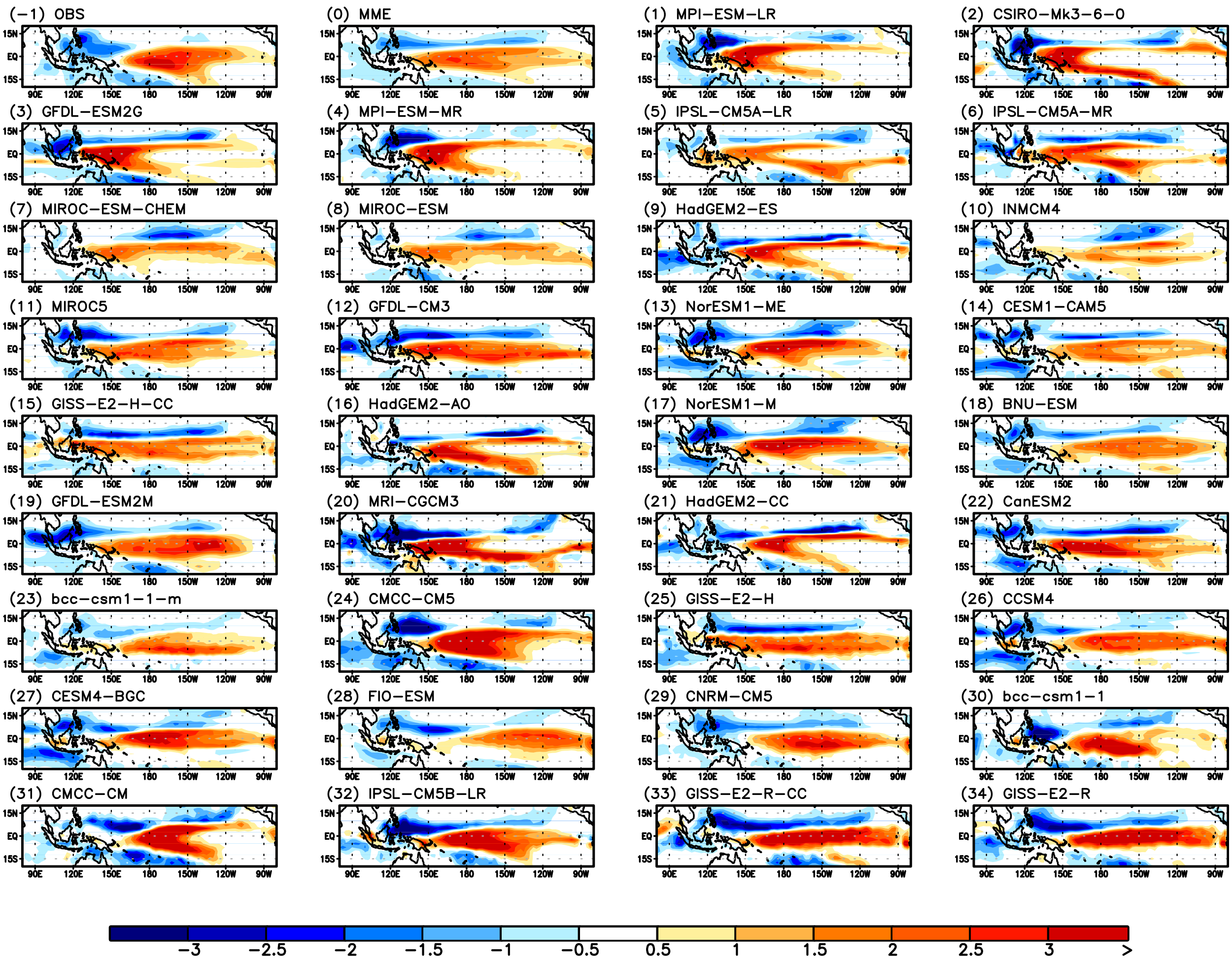

FIG. 1. The precipitation anomalies regressed onto the Niño-3.4 index during the December–February (DJF) season, in the observation (−1), multimodel ensemble (MME; 0), and each model (1–34; model numbers are given in Table 1). Note that the unit of the regression is mm day^{-1} °C^{-1}.

For the observed precipitation, we use the Global Precipitation Climatology Project (GPCP) monthly-mean precipitation data during 1979–2005, from WMO/WCRP/GEWEX (Adler et al. 2003). The observed SST data are from the National Oceanic and Atmospheric Administration (NOAA) Extended Reconstructed Sea Surface Temperature dataset version 3 (ERSST.v3b) during 1950–2005, from NOAA/OAR/ESRL (http://www.esrl.noaa.gov/psd/). The observed linear trend is also removed before analysis.

3. The intermodel differences in the ENSO-related atmospheric responses

In simulating the ENSO characteristics, there will be various systematic errors of climate models. In this study, for simplicity we focused on systematic errors in the precipitation pattern associated with ENSO. The precipitation patterns are the most important for determining not only the ENSO characteristics but also extratropical teleconnections. Figure 1 shows the precipitation anomalies regressed onto the Niño-3.4 index (i.e., SST anomalies averaged over 5°S–5°N, 170°–120°W) during the December–February (DJF) season. Note that the unit of the regression is mm day^{-1} °C^{-1}. In the observation, the positive precipitation anomalies are shown over the central Pacific, and the center of the precipitation anomalies is located slightly south of the equator (Harrison and Vecchi 1999). At the same time, there are negative precipitation anomalies over the off-equatorial western Pacific. The negative precipitation over the Southern Hemisphere is along the South Pacific convergence zone (SPCZ). Those overall features are detected somewhat in the multimodel ensemble (MME) result. However, several systematic errors are also clearly shown. First, the center of the positive precipitation anomalies is shifted to the west by about 20° longitude. This is one of the well-known systematic errors in many climate models (Wittenberg et al. 2006; Kug et al. 2008, 2012; Ham and Kug 2012; Zhang and Sun 2014). In addition, the meridional width of the positive precipitation is slightly narrower than the observed. The negative precipitation anomalies over the off-equatorial western Pacific are weaker than the observed, and also extend too much to the east. The negative precipitation along the SPCZ is also systematically weaker in the MME.

The systematic errors in individual models are generally larger than that of the MME, and these are quite diverse from model to model. For example, several models simulate positive precipitation anomalies over the western Pacific, implying that the atmospheric response during the ENSO shifts too far to the west (model numbers 1–4). On the other hand, some models simulate realistic positive precipitation centers (model numbers 24–27) and even eastward-shifting centers (model numbers 33–34). Some models simulate horseshoe patterns of the positive precipitation anomalies (model numbers 1, 2, 5, and 6), which is not clear in the observation. The spatial pattern of negative precipitation also varies from model to model. Some models simulate too strong negative precipitation over the off-equatorial central-eastern Pacific (model numbers 3, 6, 12, 20, 22, 25, 31, 33, and 34), and negative precipitation to the south of the equator is zonally elongated in many models, probably related to the bias in the SPCZ (i.e., the double ITCZ problem; Lin 2007). It should be pointed out that the ENSO-related responses of the individual models are quite different from that in the MME, meaning that the MME response does not represent the atmospheric ENSO response of the individual model. In other words, in addition to the MME response, it is worthwhile to examine the intermodel difference to increase our understanding of the simulated ENSO response.

To investigate the intermodel differences in the ENSO-related atmospheric responses, we first calculate the deviation of each model's atmospheric ENSO response from the MME (a total of 34 deviation maps). Then, we apply empirical orthogonal function (EOF) analysis, using those 34 deviation maps. This analysis provides information of the dominant intermodel differences and model uncertainties in the CMIP5 models. So, we can quantify which part of the ENSO-related atmospheric response is most difficult to simulate in the climate models. Figure 2 shows three dominant EOF eigenvectors of intermodel differences in the ENSO-related precipitation. The first EOF exhibits a positive signal over the equatorial central Pacific, whose peak is around 170°W, and a negative signal over the off-equatorial western Pacific. As the center of positive precipitation anomalies in the MME is around 170°E (shown with contours), this implies that the first EOF is associated with the zonal location difference of positive precipitation during El Niño, among the CMIP5 models. That is, in the model in which the first EOF is positively projected, the center of positive precipitation anomalies is shifted to the east compared to the MME response, presumably close to the observational one, while a negative projection of the first EOF denotes a westward shift of the El Niño–related convection anomaly, suggesting a more serious bias. In addition, the first EOF also contributes to a slight north–south shift of the negative precipitation anomalies over the western Pacific. In the same way, the second (third) EOF is associated with the southward (northward) shift of the positive convection center, during El Niño. It is obvious that the amplitude of the anomalies in the second and third EOF is weaker, than that in the first EOF.

This above analysis shows that the difference in the zonal location of the ENSO-related convection center is the most dominant of the intermodel differences in CMIP5. Before investigating the zonal shift of positive ENSO precipitation associated with the first EOF in more detail, one might want to confirm that the single dominant EOF well represents the zonal location difference among climate models. To confirm this point, the ENSO-related precipitation anomalies in each model are reconstructed by using only the first EOF; then, the center of positive precipitation anomalies is calculated, as follows:

$$X = \frac{\int \mathrm{PRCP}(x) x \, dx}{\int \mathrm{PRCP}(x) \, dx}, \tag{1}$$

where $\mathrm{PRCP}(x)$ denotes the Niño-3.4-regressed precipitation averaged over 5°S–5°N, and x denotes the longitude. Note that only the positive value of the regression remains before calculation, and the zonal integration is executed over 120°E–90°W. This definition is similar to that used in Kug et al. (2010) and Ham et al. (2013). Figure 3 denotes the center of the reconstructed and the original positive precipitation. The center of the original positive convection varies from 150°E to 160°W, and the reconstructed center mimics this variation well. The correlation coefficient between the reconstructed and original center is 0.88, confirming that the first EOF represents the intermodel differences well, in the zonal location of the ENSO-related precipitation center in CMIP5 models. The observed center is at about 170°W,

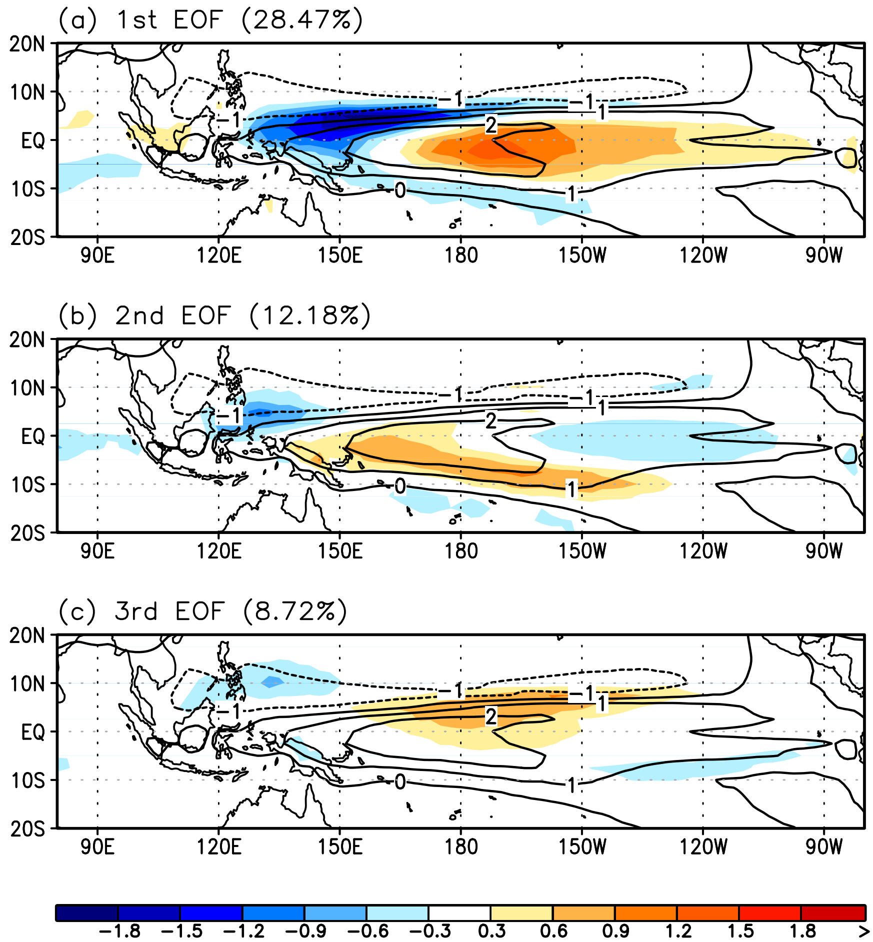

FIG. 2. The shading denotes the (a) first, (b) second, and (c) third EOF eigenvectors of intermodel differences (i.e., deviation of the individual model's response from the MME) in the ENSO-related precipitation. The contour denotes the MME response of the ENSO-related precipitation.

implying that most of the models simulate westward-shifting convection anomalies, while several models (model numbers 24–33) simulate realistic center locations.

The zonal shift of the ENSO-related convection centers in CMIP5 models is dynamically coupled to the change in the ENSO-related circulation and SST. Figure 4 shows the regression coefficients between the first EOF principal component (PC), corresponding to the dominant eigenvector shown in Fig. 2a, and intermodel differences of the Niño-3.4-regressed 850-hPa zonal wind and SST. Note that only the values above the 95% confidence level are shown, using the *t* test of the correlation coefficient. The MME low-level zonal wind response during ENSO shows westerly anomalies over the equatorial western Pacific and easterly anomalies over the Indian Ocean and Maritime Continent (contour in Fig. 4a). Consistent with the positive precipitation signal over the central Pacific in the first EOF, the first EOF-regressed zonal wind anomalies exhibit the westerly over the central Pacific. The negative precipitation anomalies over the western Pacific in first EOF are also consistent with the local easterly. The precipitation and zonal wind anomalies are zonally in phase, as pointed out in previous studies (Clarke 1994). In short, the positive projection of the first EOF denotes that the westerly over the central Pacific intensifies, and the easterly over the Maritime Continent extends to the western Pacific.

The signal in the SST is also dynamically connected to that in the precipitation and the zonal wind. As the amplitude of Niño-3.4 on the regression is normalized to have the anomalies per degrees Celsius in all models, there is no signal over the eastern Pacific. Between the western Pacific easterly and central Pacific westerly (i.e., low-level divergence zone), there is a negative SST signal around 150°E–180°. Because the MME of the ENSO

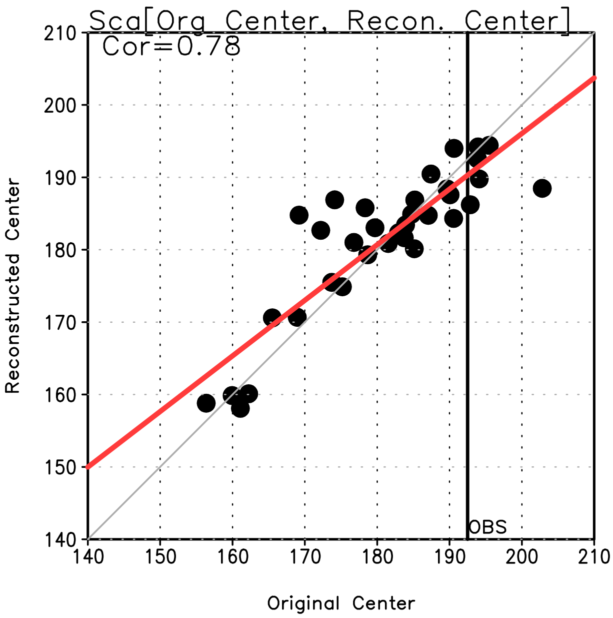

FIG. 3. The zonal center of the original (x axis) and the reconstructed (y axis) positive precipitation during El Niño, in 34 CMIP5 models. The observed zonal center is denoted as a red line.

SST exhibits a positive anomaly in this region, the positive projection of the first EOF confines the El Niño–related positive SST anomalies to the east, which is realistic.

Is this intermodel difference corresponding to the first EOF related to the mean states? To answer this question, Fig. 5 shows the correlation between the first EOF PC and the intermodel difference of the climatological precipitation, 850-hPa zonal wind, and SST during the DJF season. For this, the deviation of each model's climatology from the MME is obtained, and then the correlation with the first EOF PC is calculated. Note that the period to define the climatology is from 1950 to 2005. In the precipitation, there is a strong positive correlation over the equatorial central Pacific, implying that the climate models with a positive projection of the first EOF tend to have wetter climatology over the equatorial region than the MME climatology. That is, the models whose ENSO-related convection anomalies are shifted to the east, compared to that of the MME, have wetter climatology over the central Pacific than that of the MME. This result is consistent with previous studies that the dry climatology over the equatorial central-eastern Pacific confines the ENSO-related convection to the western Pacific (Kim et al. 2011a; Ham and Kug 2012; Watanabe et al. 2011). This study confirms their findings in more rigorous ways using multimodel CMIP5 output. In addition to the wetter signal over the equatorial central Pacific, there is a dry signal over the off-equatorial western Pacific, South Pacific, and Maritime Continent, where the negative anomalies exist in the first EOF mode.

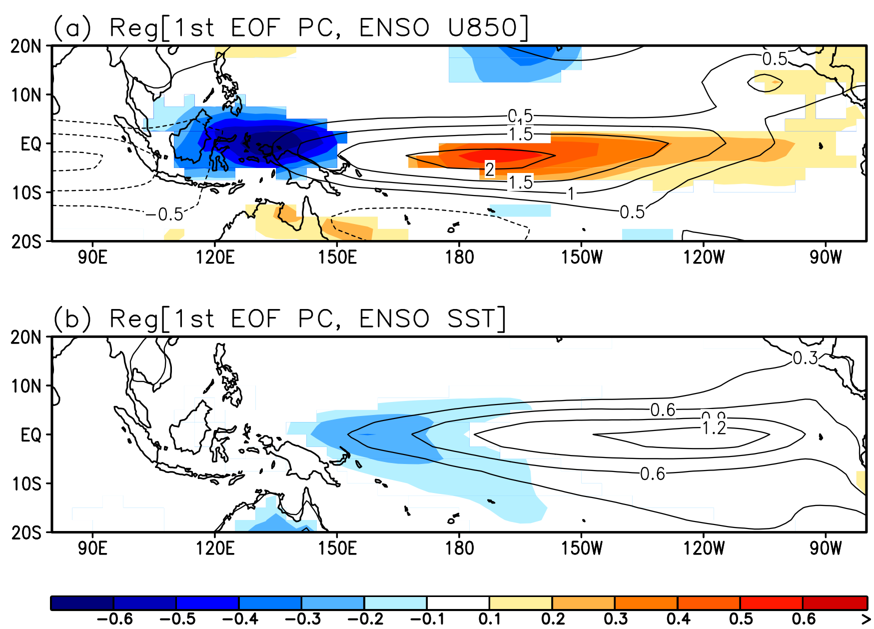

FIG. 4. The shading denotes the regression coefficients between the first EOF principal component (PC), corresponding to the dominant eigenvector shown in Fig. 2a, and intermodel differences of the Niño-3.4-regressed (a) 850-hPa zonal wind and (b) SST. The contour denotes the MME response of the 850-hPa zonal wind and SST, respectively, regressed onto the Niño-3.4 index.

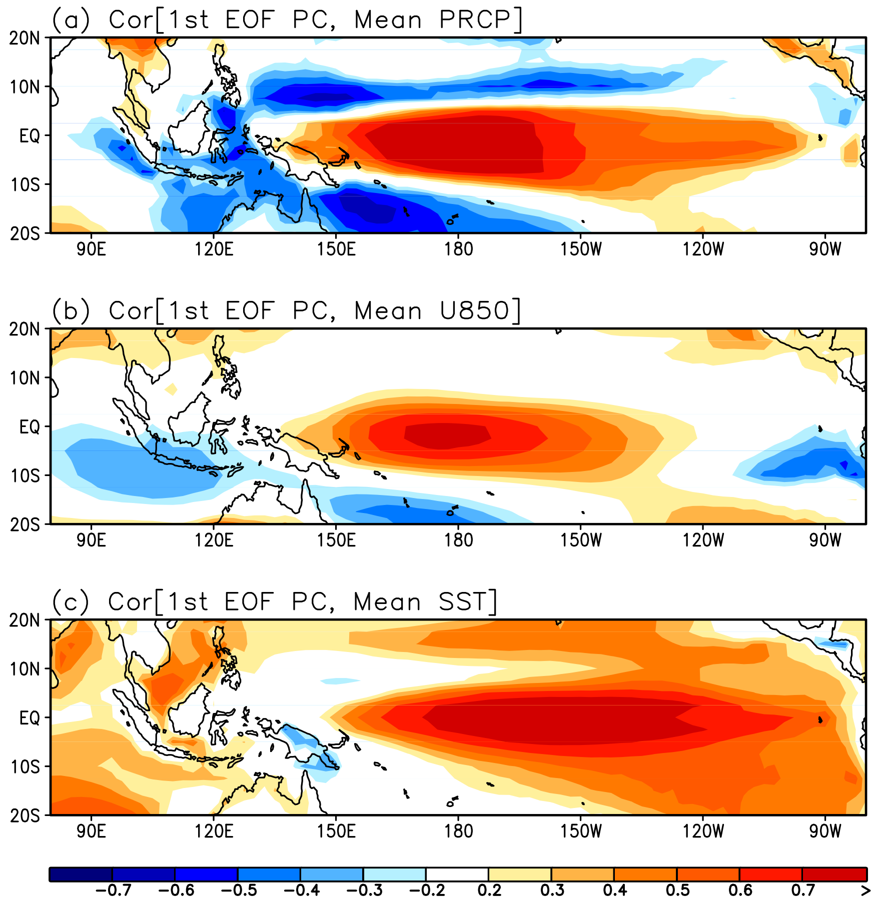

FIG. 5. The correlation between the first EOF PC, and the intermodel difference of the (a) climatological precipitation, (b) 850-hPa zonal wind, and (c) SST, during the DJF season.

In short, the positive projection of the first EOF implies that climate models with wetter climatology allow a large precipitation response to the ENSO SST forcing over the central Pacific, while the dry climatology over the off-equatorial western Pacific is associated with stronger negative ENSO-related anomalies over that region. On the other hand, a negative projection of the first EOF means that the dry climatology over the equatorial central Pacific forces the ENSO-related convection center to shift to the west. Consistent with climatological precipitation, the low-level climatological zonal wind shows a westerly signal over the central Pacific, with warmer climatological SST. The maximum correlation coefficient between EOF PC and the basic states is over 0.7 in SST, precipitation, and 850-hPa zonal wind, which means that this relationship is quite robust and significant.

It is found that the differences in the mean state and the ENSO-related atmospheric response among climate models can also modify the ENSO evolution properties. To examine the difference in the ENSO evolution according to the projection amplitude of the first EOF, we first calculate the lagged regression of the intermodel differences of the equatorially averaged (5°S–5°N) ENSO-related SST anomalies onto the first EOF PC, similar to Fig. 4; then, it is added (i.e., MME + regression) or subtracted (MME − regression) to the MME response of the ENSO-related SST anomalies from the preceding January and subsequent December of the ENSO peak season (Fig. 6). Note that the result in the MME + regression (MME − regression) is quite similar to the result with the composite of models whose first EOF PC is positive (negative). For the comparison, the ENSO evolution in the observation is also shown.

The observed ENSO evolution shows stationary evolution to a large extent, while it shows weak eastward propagation before the ENSO peak, which resembles an El Niño's evolution after the 1980s (An and Wang 2000; Choi et al. 2011; Boucharel et al. 2013). A weak negative SST signal related to the phase transition of ENSO is shown after a +9-month lag. Interestingly, the models with the positive projection of first EOF simulate

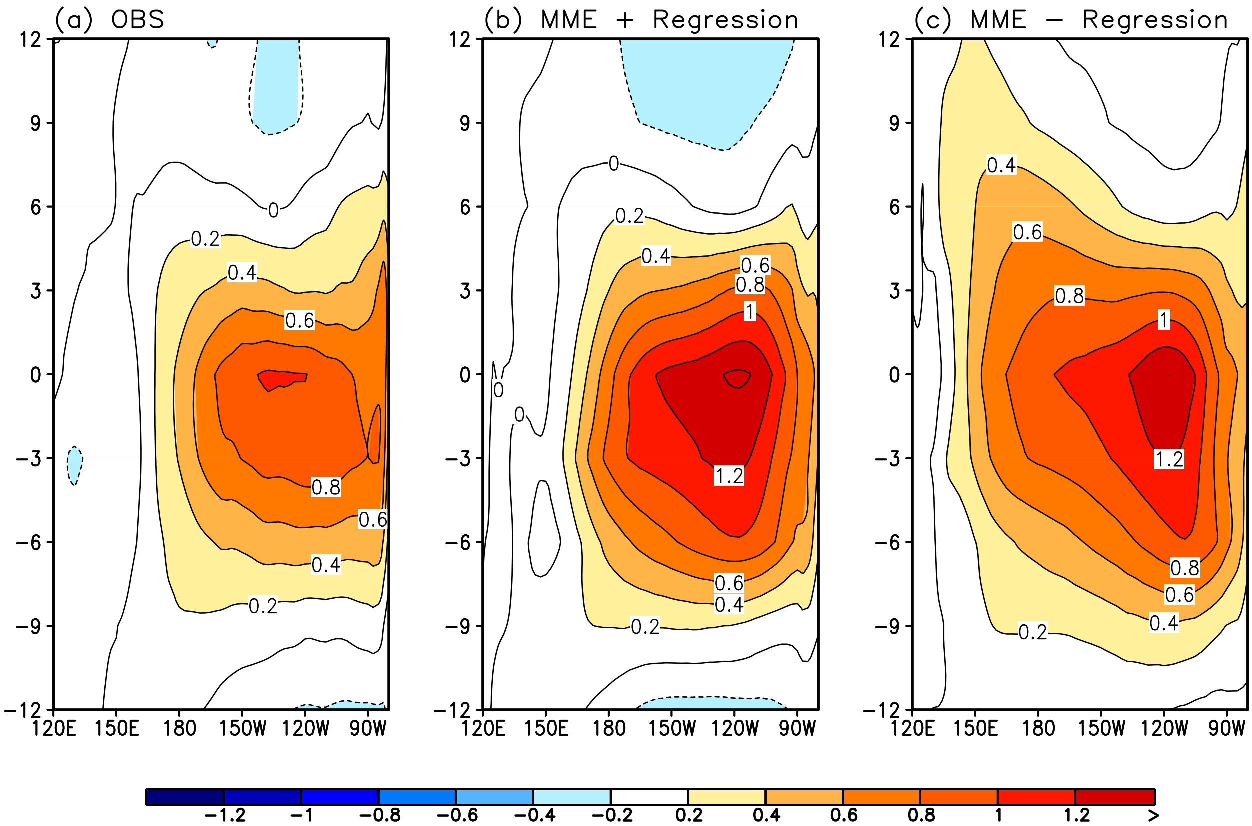

FIG. 6. (a) The observed equatorially averaged (5°S–5°N) ENSO-related SST anomalies from the preceding January (i.e., −12 on the y axis), to subsequent December (i.e., +12 on the y axis) of the ENSO peak season. Also shown is the regression of the intermodel differences of the equatorially averaged ENSO-related SST anomalies onto the first EOF PC from the preceding January to subsequent December of the ENSO peak season, which is (b) added to and (c) subtracted from the MME response of the Niño-3.4-regressed SST.

realistic ENSO propagation and decay in addition to the DJF precipitation response. When the first EOF is positively projected (i.e., MME + regression), the positive SST anomalies weakly propagate from the western to the eastern Pacific (i.e., eastward propagation). On the other hand, when first EOF is negatively projected (i.e., MME − regression), there is clear westward propagation of the positive SST anomalies. According to the recent studies of Santoso et al. (2013), the propagation feature of the ENSO SST can be determined by the strength of the climatological zonal current. They found that the westward propagation of the ENSO SST is associated with the stronger mean westward current. When the mean westward current weakens, the westward propagation of the ENSO SST becomes prominent. Consistent with their argument, the models with negative projection of the first EOF, which is associated with the westward propagation of the ENSO, tend to have stronger mean easterly trade winds (the opposite pattern to Fig. 5b) and stronger mean westward currents. The other interesting point is that there are weak negative SST signals at −12- and 9-month lags in the MME + regression map, suggesting that the ENSO transition is faster in the model with positive projection of the first EOF. Consistent with previous studies, the stronger ENSO-related easterly anomalies over the western Pacific, as shown in Fig. 4a, can act to excite an upwelling Kelvin wave, to lead to a faster transition to La Niña (Kug and Kang 2006; Kug et al. 2006).

In this section, by applying the EOF analysis to each model's deviation map from the MME, it is found that the dominant intermodel differences of the ENSO-related precipitation anomalies are related to the zonal shift of the maximum precipitation during El Niño. The first EOF of intermodel differences has positive (negative) signal to the east (west) of the MME response, implying that the positive projection of the first EOF denotes the eastward shift of the convection center. As the MME response systematically simulates the ENSO convection center shifted to the west, the positive projection of the first EOF is associated with the realistic ENSO response. The first EOF is closely linked to the differences in the mean state; that is, it is associated with the wet climatology over the equatorial central Pacific.

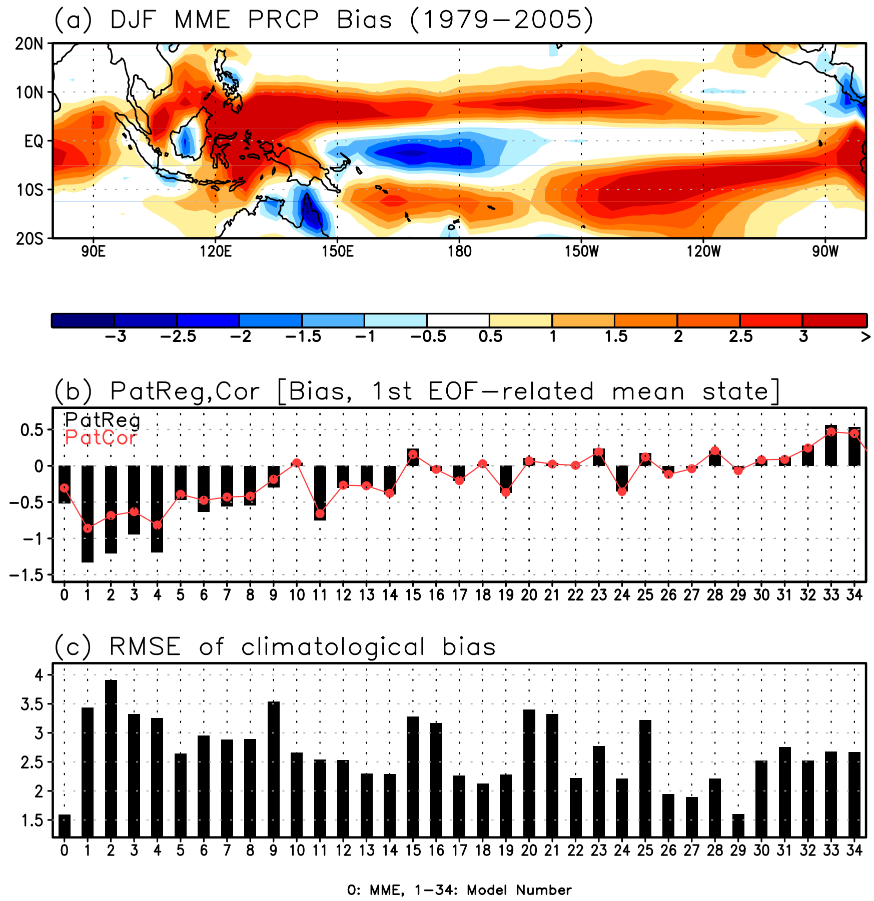

FIG. 7. (a) The climatological MME bias in the DJF precipitation, and (b) the pattern regression (black bars) and correlation (red line) of MME (0 on the *x* axis) and each model's (1–34 on the *x* axis) bias, onto the first EOF-related mean state. (c) The RMSE of climatological bias. Note that the observed precipitation climatology is based on the 1979–2005 period.

The mean state in the SST and low-level zonal wind are dynamically consistent with the precipitation. Based on those results, the following question naturally arises: Do the models with the mean state associated with the positive projection of the first EOF have a more realistic climatology than the other models? To answer this question, we will start the next section by investigating the climatological bias.

4. The improvement of ENSO systematic error through mean bias correction

Figure 7 shows the climatological MME bias in the DJF precipitation, which shows the dry bias over the equatorial western-central Pacific and wet bias over the off-equatorial regions and equatorial western Pacific. This pattern is also consistent with Lin (2007) with CMIP3 data. The spatial pattern of the MME precipitation bias tends to be opposite to that of the first EOF-related mean state. This indicates that the positive projection of the first EOF tends to compensate for the systematic error related to the MME bias. For example, the equatorial dry MME bias over the equatorial western-central Pacific is compensated by the equatorial positive signal in the climatological associated with the first EOF, as shown in Fig. 5a. Similarly, the wet MME biases over the off-equatorial regions are cancelled by the off-equatorial negative signal in the mean state, coupled to the first EOF. As a result, the pattern regression between the mean state coupled to the first EOF, and each mode's bias, is generally negative (Fig. 7b); the pattern regression of the MME is −0.53. This implies that climate models with a positive projection of the first EOF tend to have a smaller precipitation bias as shown in Fig. 7c, in addition to smaller ENSO-related precipitation errors, as shown in the previous section.

As a better climatological precipitation tends to guarantee a more realistic ENSO precipitation response, one can imagine how the ENSO precipitation response in climate models would be improved when the climatological precipitation bias is diminished. In this aspect, we can correct the climatological precipitation in a statistical way, and then examine how much the ENSO precipitation response is improved. The statistical correction method is based on a simple linear regression, as follows:

$$\mathrm{ENSO}_{\mathrm{CORR}_k} = \mathrm{ENSO}_{\mathrm{ORG}_k} - \sum_{i=1}^{N} \alpha_{i,k}\mathrm{EOF}_i, \quad (2)$$

$$\alpha_{i,k} = \frac{\sum_{x,y}^{\mathrm{Pacific}} [M_i \mathrm{Bias}_k]}{\sum_{x,y}^{\mathrm{Pacific}} [M_i]^2}, \quad \text{and} \quad (3)$$

$$M_i = \frac{\sum_{k=1}^{\mathrm{Nm}} [C_k \mathrm{EOF\_PC}_{i,k}]}{\sum_{k=1}^{\mathrm{Nm}} [\mathrm{EOF\_PC}_{i,k}]^2}, \quad (4)$$

where $\mathrm{ENSO}_{\mathrm{CORR}_k}$, $\mathrm{ENSO}_{\mathrm{ORG}_k}$, and EOF_i are the ENSO-related precipitation anomalies after the statistical correction and before the correction of the kth model and the ith EOF eigenvector shown in Fig. 2, respectively. Also, M_i is the spatial distribution of the regression coefficient of the intermodel difference of the DJF precipitation climatology (C_k) with respect to the ith EOF PC time series ($\mathrm{EOF\_PC}_{i,k}$) (e.g., Fig. 5a). Note that k is a model number, and Nm is the total number of models, which is 34 in this study. The correction for the kth model is done by multiplying the coefficient $\alpha_{i,j}$, which is defined as the pattern regression between M_i, and the mean precipitation bias in the kth model (Bias_k). We utilized 10 dominant EOF modes (i.e., N is 10 in this study). The general result in this paper is not much dependent on the number of EOF modes once it is over 10 or so because the explained variance of the 10th EOF is less than 2%; therefore, the contribution of minor EOFs than 10th EOF is ignorable even if M_i were quite similar to the climatological bias. The pattern regression is done within the Pacific basin (15°S–15°N, 80°E–90°W) to focus on the equatorial variability. Assuming only first EOF is used for the correction, the pattern of M_1 (i.e., Fig. 5a) is negative projected onto MME bias field (i.e., Fig. 7a), and the model-averaged $\alpha_{1,k}$ (i.e., $\sum_{k=1}^{\mathrm{Nm}}\alpha_{1,k}$) is negative (i.e., -0.52). Simply, this number is multiplied to the first EOF (i.e., Fig. 2a) and then subtracted from the original ENSO response (i.e., $\mathrm{ENSO}_{\mathrm{ORG}}$) to make a correction (i.e., $\mathrm{ENSO}_{\mathrm{CORR}}$). As a result, the projected amplitude of first EOF onto $\mathrm{ENSO}_{\mathrm{CORR}}$ is increased to 1.37 from 0.80 in $\mathrm{ENSO}_{\mathrm{ORG}}$, which becomes similar to the observed projection amplitude (i.e., 1.66).

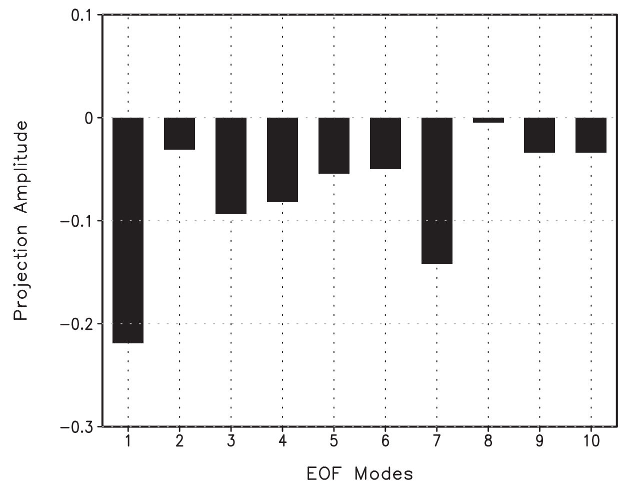

FIG. 8. The pattern projection of the MME bias onto each EOF.

This algorithm is to correct the ENSO-related atmospheric response by using the linear relationship between the intermodel differences in the mean state and the ENSO response. The bias projected onto the dominant EOFs is linearly removed to correct the ENSO-related precipitation anomalies. According to this formulation, if, for example, the climatological bias of the 10th model were completely opposite to the first EOF-related mean state (M_1), only $\alpha_{1,10}$ would have negative values, to correct the original ENSO response. On the other hand, if the amplitude of bias projected on the EOF mode-related mean state (M_i) were small, that would lead to a small correction, as $\alpha_{i,j}$ is small. Note that this statistical method only utilizes the intermodel differences of climatological bias and ENSO-related precipitation to make a correction, and no prior information about the targeted field (i.e., the observed atmospheric ENSO response) is given.

Figure 8 shows the pattern projection of MME bias onto each EOF (i.e., equivalent to MME of $\alpha_{i,j}$), to examine the contribution of each EOF to the statistical correction method. As shown in Fig. 7b, the spatial pattern is generally opposite between the first EOF-related mean state and the MME bias; therefore, the contribution of the first EOF is relatively larger than that of the other EOFs. The contribution of each EOF is smaller for higher modes; however, it is interesting that the contribution of the seventh EOF is quite large. Please note that the small explained variance of the minor EOFs is for intermodel differences (i.e., differences between an individual model and the MME), which does not necessarily guarantee the small

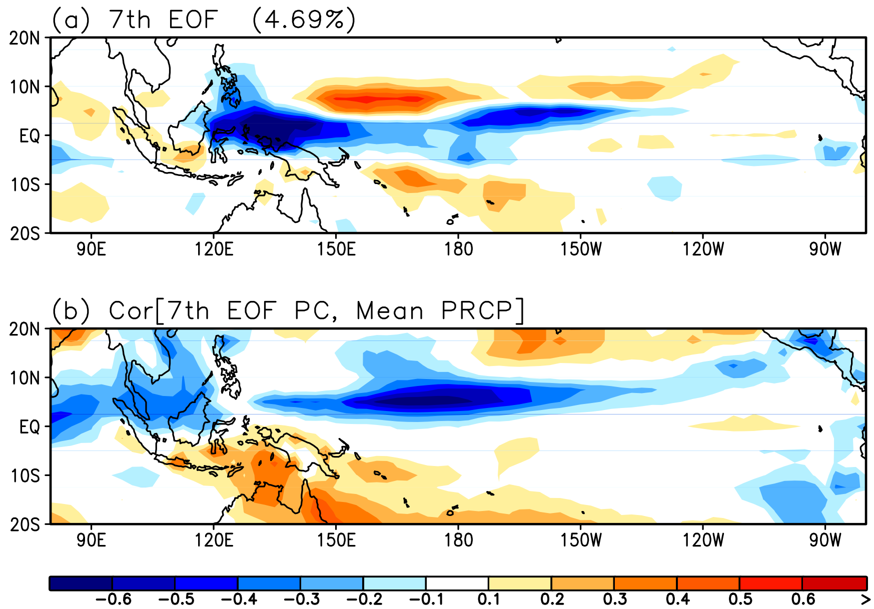

FIG. 9. (a) The seventh EOF of the intermodel differences in the ENSO-related precipitation. (b) The correlation between the seventh EOF PC and the intermodel difference of the climatological precipitation (i.e., as in Fig. 5a, but with the seventh EOF).

contribution of minor EOFs onto the climatological bias (i.e., the difference between an individual model and observation).

To investigate the contribution of the seventh EOF in more detail, Fig. 9 shows the seventh EOF and the correlation between the seventh EOF PC. The result shows that the seventh EOF is related to the distribution of equatorial and off-equatorial precipitation anomalies (Fig. 9a). Further, this intermodel difference is associated with climatological precipitation over the off-equatorial western and central Pacific. That is, the seventh EOF shows that the off-equatorial precipitation during El Niño is related to the local mean precipitation. In other words, the model with a wetter ITCZ can lead to stronger local positive precipitation anomalies (or, a dryer ITCZ is linked to stronger local negative precipitation anomalies). As the negative mean precipitation signal over the off-equatorial western and central Pacific is opposite to the MME precipitation bias, the seventh EOF is therefore negatively projected onto the MME precipitation bias. According to the algorithm, in the model with dry bias over the off-equatorial western and central Pacific, the statistical correction using the seventh EOF acts to enhance the negative precipitation anomalies over the western Pacific.

Figure 10 shows the precipitation response during the ENSO in the observation, the MME, and the MME after the statistical correction. Note that the observed and the original MME responses are the same, as shown in Fig. 1. In the observation, the positive precipitation anomalies over the equatorial central Pacific are between 180° and 170°W. The center of the positive precipitation is slightly to the south of the equator, and the amplitude is about 3 mm day^{-1} °C^{-1}. The amplitude of the negative precipitation anomalies over the western Pacific is between −1.5 and −2 mm day^{-1} °C^{-1}, and the center is located over the off-equatorial Northern Hemisphere. The negative precipitation anomalies along the SPCZ are also clear. In the MME, the positive precipitation center shifts to the west, and the maximum amplitude is weaker than the observed. In addition, it is too much zonally elongated, and the meridional width is narrower than the observed. The negative precipitation anomalies over the western Pacific are weaker and extend too far to the east. Also, the negative precipitation along the SPCZ is systematically weaker.

After the correction, those deficiencies listed above are distinctively improved. The center of the positive precipitation anomalies shifts to the east, compared to that of the original MME response, and the zonal location of the positive precipitation center becomes similar to the observed. Also, it is to the south of the equator, as in the observed. The amplitude is also increased, to reach 3 mm day^{-1} °C^{-1} at peak location. The amplitude of the negative precipitation over the off-equatorial western Pacific is intensified over −2 mm day^{-1} °C^{-1}, after the correction. In addition, the positive precipitation anomalies over the western Pacific shrink

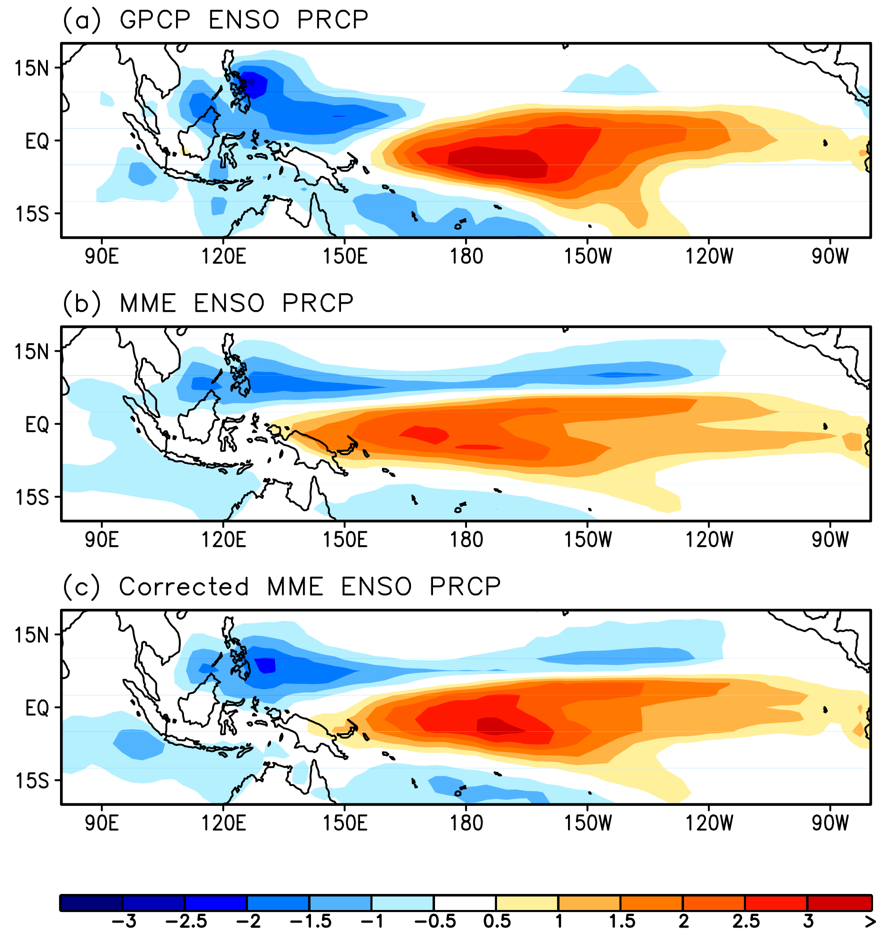

FIG. 10. The precipitation response during the ENSO in the (a) observation, (b) MME, and (c) MME after the statistical correction.

relatively to the east, after the correction, while the MME shows that the positive precipitation anomalies extend too far to the west. The negative precipitation anomalies along the SPCZ are also intensified. As shown in Fig. 8, the contribution of the first EOF is largest, and it especially acts to correct the zonal location of positive precipitation anomalies related to the ENSO. The third EOF contributes to widening the meridional width of the positive convection center (not shown). The amplitude of the negative precipitation over the off-equatorial western Pacific seems to be mainly corrected by the first and seventh EOFs. The pattern correlation between the observed and the MME after the correction over the tropical Pacific basin (15°S–15°N, 80°E–90°W) is 0.92; while that between the observed and the original MME was 0.81. This implies that the correction of the climatology can improve the ENSO simulations.

As well as the MME response, it is worthwhile to examine the individual model's pattern after the correction. Figure 11 shows the pattern correlation between the observed and the simulated ENSO precipitation responses before (gray) and after the correction (red) in each model. The model number is the same as in Fig. 1, and note that it is a low order of the first EOF PC. That means that the original atmospheric ENSO response in the model with low numbers shifts to the west, compared to the observed. Before the correction, the pattern correlation varies between 0.3 and 0.8. It is clear that after the correction, the pattern correlations in most of the climate models are distinctively improved. After the correction, the pattern correlation in most climate models is higher than 0.6. It is interesting that the improvement after the correction in the model with low numbers tends to be higher than the others. For example, the pattern correlation of the original response of the model number 1 is lower than 0.3; however, that after the correction is over 0.7. This implies that the models with larger bias and systematic error tend to be much more beneficial to the correction than the others.

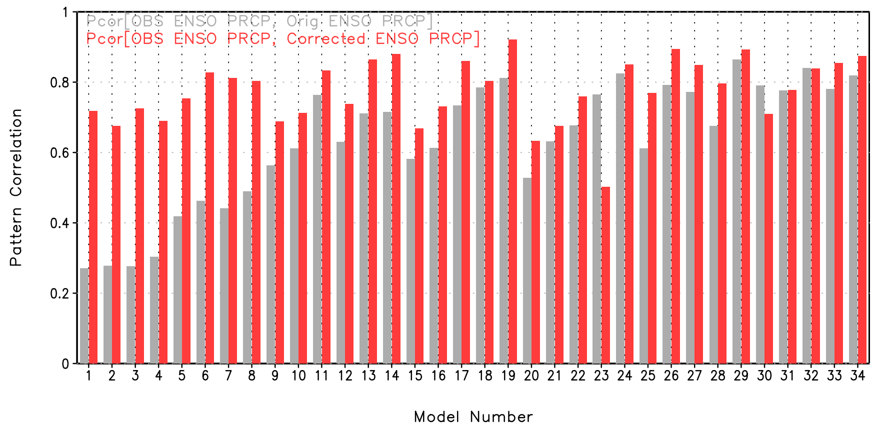

FIG. 11. The pattern correlation between the observed and the simulated ENSO precipitation response before (gray bars) and after the correction (red bars), in each model.

To examine this point in more detail, Fig. 12 shows the scatter diagram between the pattern correlation between the observed and simulated response, before and after the correction, in all models. Note that the color of each dot corresponds to the first EOF PC. As mentioned in the previous paragraph, the pattern correlation after the correction is above 0.6, except for one model, while one-third of the model's original response is below 0.6. Except for two models, the statistical correction proposed in this study improves the atmospheric ENSO responses in climate models. In addition, it is clearly shown that after the correction, the model with low number (i.e., low first EOF PC) tends to improve much more than the others. In models with first EOF PC lower than −1.8, the improvement after the correction is about 0.4. When the first EOF PC is between −1.8 and −1.2, the original pattern correlation is slightly larger than 0.4, while the corrected pattern correlation is about 0.8, so that there is roughly an improvement of 0.4. On the other hand, in the models whose first EOF PC is small or positive, the improvement after the correction is about 0.1–0.2, which is systematically smaller than the models with low first EOF PC. However, as their pattern correlation was high before the correction, the pattern correlation after the correction is similar for all models. In short, there is distinctive improvement in simulating the atmospheric ENSO response after the statistical correction in most climate models, and the improvement is robust for the models whose original ENSO atmospheric response was far from realistic.

5. Concluding discussion

In this study, the dominant intermodel differences (i.e., deviations from the MME) in the simulated atmospheric ENSO responses, and their relationship with climatological state, are investigated, using CMIP5 models. It is found that the dominant intermodel difference of the ENSO precipitation in CMIP5 models is associated with the zonal location of the positive precipitation center during El Niño. The first EOF shows the positive (negative) values to the east (west) of the MME response, indicating that the positive projection of the first EOF shifts the atmospheric ENSO response to the east compared with the MME response. The coupled pattern to the first EOF shows an additional westerly

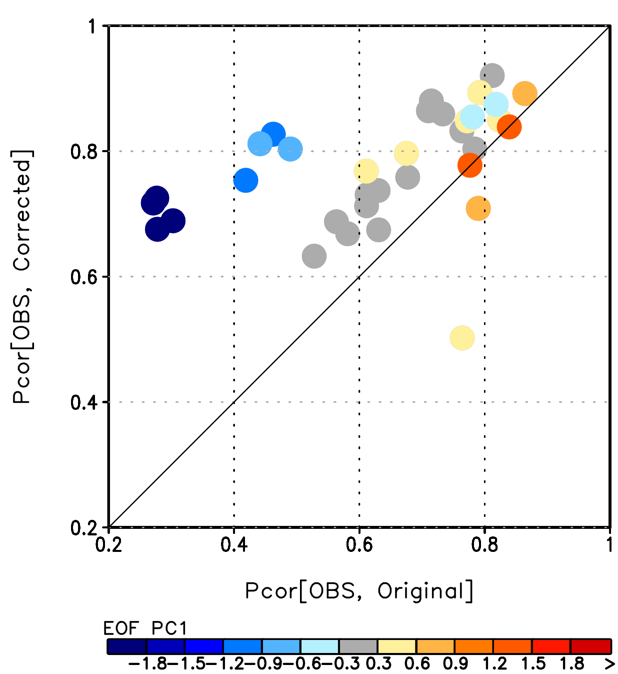

FIG. 12. The scatter diagram between the pattern correlation between the observation and simulated response before (x axis) and after the correction (y axis), in all models. Note that the first EOF PC is shaded.

(easterly) at the location of the enhanced (reduced) precipitation. As the MME response exhibits a westward-shifted response, with extension of positive ENSO SST to the western Pacific compared with the observed, the model simulation becomes realistic when the first EOF is positively projected.

It is found that this dominant intermodel difference in the ENSO response is strongly correlated with the differences in the basic state. The models with wetter climatology than the MME climatology over the central Pacific tend to shift positive ENSO precipitation anomalies to the east (i.e., positive projection of the first EOF). As the models tend to have dry bias over the equator, the models with wetter climatology than the MME have realistic climatology. The correlation between the first EOF PC and intermodel difference of mean precipitation during the DJF season is over 0.7, implying that this relationship is quite robust. Consistent with wet climatology over the central Pacific, the models whose ENSO response is shifted to the east exhibit warmer SST climatology over the eastern Pacific, and a stronger low-level westerly over the central Pacific, than the MME.

Those intermodel differences in the ENSO response and climatology also lead to different ENSO periods and propagations. The models that are positively projected onto the first EOF tend to have shorter ENSO periods, which resembles the observation, than the models that are negatively projected. This might be related to the stronger ENSO-related easterly over the Maritime Continent, leading to faster transition of the ENSO. In addition, a weaker mean easterly (i.e., stronger eastward) current over the central Pacific in the models with positive projection of the first EOF might lead to an eastward propagation of the ENSO SST. On the other hand, the models that are negatively projected onto the first EOF are associated with longer periods of the ENSO, with westward propagation.

A statistical correction of the ENSO response by minimizing the mean bias is developed by utilizing the strong relationship between the mean state and the atmospheric ENSO response. As the models with better climatological states tend to simulate more realistic atmospheric ENSO responses, this statistical method to correct the mean bias mostly improves the ENSO response. After the statistical correction, the deficiencies in simulating the MME ENSO precipitation are, to some extent, compensated for. The center of positive precipitation related to El Niño shifts to the southeast, and the negative precipitation over the off-equatorial western Pacific and along the SPCZ becomes stronger, which becomes realistic. The pattern correlation of atmospheric MME response increases from 0.81 before the correction to 0.92 after the correction over the tropical Pacific basin. As well as the MME response, there is a clear improvement of the individual model's ENSO response. In particular, this improvement is robust in the models whose original response is far from realistic. That is, the improvement in the pattern correlation between the observed and the simulated is about 0.4 in the models with relatively large errors in the climatological precipitation and ENSO response, whereas it is between 0.1 and 0.2 in the models with relatively small errors. This study supports the arguments in previous studies that a realistic climatology guarantees better interannual variability (Fennessy et al. 1994; Sperber and Palmer 1996; Kang et al. 2002; Lee et al. 2010). While previous studies focused on finding this relationship, this study further introduces a methodology to utilize this relationship for improving the model simulation. Insofar as a more realistic climatology tends to be linked to better interannual variability, it is obvious that the statistical correction introduced in this study leads to an improvement of the simulation quality.

As this statistical method does not include any prior information about the targeted field (i.e., the observed ENSO precipitation response in this study), this method can therefore be applied to the climate change response. O'Gorman (2012) showed that the model-simulated response of tropical precipitation extremes to interannual climate variability in current climate is strongly correlated with their response to longer-term climate change. This implies that the relationship between two different time scales in current climate can be successfully extrapolated to the relationship between current climate and climate change. In addition, there are some clues that the current climate condition is closely linked to the climate change that the changes in the precipitation after the climate change is greater as the current climatology is wetter, and weaker as the current climatology is drier (i.e., ''wet gets wetter, and dry gets drier'' response) (Knutson and Manabe 1995; Held and Soden 2006; Wentz et al. 2007; Chou et al. 2013). Based on those studies, this method might provide clues to deduce some convincing conclusion on climate sensitivity using climate models.

One can wonder about the possible implication of the proposed method to address the two types of El Niño events (Ashok et al. 2007; Kao and Yu 2009; Kug et al. 2009; Yeh et al. 2009). It seems that the zonal phase differences of El Niño response, which is a key feature in whether the model can simulate two equilibrium states of the El Niño, can be also influenced by the mean state. Based on the previous studies of Ham and Kug (2012), it is shown that the independence of the two types of El Niño events is quite different from model to model, and is significantly correlated with the climatological wetness over the equatorial central-eastern Pacific. As the climatological precipitation over the equatorial central-eastern Pacific is increased, the independence of the two types of El Niño events tends to increase. As most of models tend to underestimate the independence between two types of El Niño events (i.e., present a single type of El Niño) and indicate drier equatorial wetness than the observed, the application of this statistical correction method would help to simulate realistic independence between two types of El Niño in climate models.

In addition, this can also be applied to the multimodel dynamical forecast dataset by the North American Multimodel Ensemble (NMME) project (Kirtman et al. 2014), or EUROSIP (http://old.ecmwf.int/products/forecasts/seasonal/documentation/eurosip/ch3.html). The basic idea is to replace the ENSO-related component in the prediction to the corrected pattern. First, the spatial pattern of the ENSO-related precipitation is calculated in each prediction system; then the corrected ENSO-related precipitation is obtained using the proposed method in this study. Once this relationship is obtained, the predicted precipitation pattern regressed onto the original ENSO pattern is replaced to the corrected ENSO pattern. Based on studies suggesting that the seasonal forecast skill is proportional to the simulation quality in the climatology over the tropics (Lee et al. 2010; Ham et al. 2012), it is probable that the application of the proposed method to the operational forecast system would improve the forecast skills. Also, this method has some advantages, in being applied to forecast data. As the proposed statistical method only requires a climatological bias, which is not very sensitive to the validation method (or slight change of number of samples), this method is free from the overfitting problem. Therefore, it can provide a stable solution without sudden differences between the training and forecast period. As well as the prediction skill over the tropics, it can also improve the prediction quality over the midlatitude climate, with the aid of realistic teleconnections.

However, it should be noted that this method would not always improve the simulation quality when an unrealistic climatology is linked to a better simulation of the variability. For example, Kim et al. (2011b) showed that a model with realistic climatological precipitation failed to simulate a realistic eastward propagating MJO signal. In this case, the statistical correction based on the quality of the climatological state might worsen the MJO simulation quality. Therefore, before applying this method to other targets, careful analysis should be conducted.

The EOF analysis to diagnose the dominant intermodel differences is easy to apply and can be a powerful tool to understand the simulation quality in current climate models. It might be especially useful when the spatial pattern of systematic errors is diverse among climate models. With the analysis tool introduced in this study, we can easily categorize systematic errors in high order of explained variance, to focus on the dominant errors. In addition, as the number of models we can utilize is expected to increase, such a categorization would be essential in the future. Otherwise, we have to compare the individual model's response one by one to examine the systematic errors in climate models. This is an important issue, as the MME response obviously does not represent the individual model's response (e.g., Fig. 1); also, this is essential to providing directions to the climate modeling community, to improve the quality of climate models, in terms of both climatology and variability.

In addition, this study can boost the climate community's unequivocal demands for the multimodel dataset, by maximizing its application. First, the relationship between intermodel diversity in the interannual variability and mean state will become much more robust and clearer, as the number of utilized models is increased; and this implies that the model simulation can be highly reliable, by using as many models as possible. Second, by not just taking an average of multimodel output to cancel out the systematic errors, this study shows that the individual model's spatial error pattern from the MME also contains important information that is worthwhile to utilize. Therefore, this study can accelerate the need of huge international collaborations like CMIP, to reach a solid conclusion for worldwide climate information users.

Acknowledgments. This study is supported by Chonnam National University, 2013.

REFERENCES

AchutaRao, K., and K. R. Sperber, 2006: ENSO simulation in coupled ocean–atmosphere models: Are the current models better? *Climate Dyn.*, **27,** 1–15, doi:10.1007/s00382-006-0119-7.

Adler, R. F., and Coauthors, 2003: The Version-2 Global Precipitation Climatology Project (GPCP) monthly precipitation analysis (1979–present). *J. Hydrometeor.,* **4,** 1147–1167, doi:10.1175/1525-7541(2003)004<1147:TVGPCP>2.0.CO;2.

An, S.-I., and B. Wang, 2000: Interdecadal change of the structure of the ENSO mode and its impact on the ENSO frequency. *J. Climate,* **13,** 2044–2055, doi:10.1175/1520-0442(2000)013<2044:ICOTSO>2.0.CO;2.

——, Y.-G. Ham, J.-S. Kug, A. Timmermann, J. Choi, and I.-S. Kang, 2010: The inverse effect of annual-mean state and annual-cycle changes on ENSO. *J. Climate,* **23,** 1095–1110, doi:10.1175/2009JCLI2895.1.

Annamalai, H., and P. Liu, 2005: Response of the Asian summer monsoon to changes in El Niño properties. *Quart. J. Roy. Meteor. Soc.,* **131,** 805–831, doi:10.1256/qj.04.08.

——, K. Hamilton, and K. R. Sperber, 2007: The South Asian summer monsoon and its relationship with ENSO in the IPCC

AR4 simulation. *J. Climate,* **20,** 1071–1092, doi:10.1175/JCLI4035.1.

Ashok, K., S. K. Behera, S. A. Rao, H. Weng, and T. Yamagata, 2007: El Niño Modoki and its possible teleconnection. *J. Geophys. Res.,* **112,** C11007, doi:10.1029/2006JC003798.

Bejarano, L., and F.-F. Jin, 2008: Coexistence of equatorial coupled modes of ENSO. *J. Climate,* **21,** 3051–3067, doi:10.1175/2007JCLI1679.1.

Bellenger, H., and Coauthors, 2014: ENSO representation in climate models: From CMIP3 to CMIP5. *Climate Dyn.,* **42,** 1999–2018, doi:10.1007/s00382-013-1783-z.

Boucharel, J., A. Timmermann, and F.-F. Jin, 2013: Zonal phase propagation of ENSO sea surface temperature anomalies: Revisited. *Geophys. Res. Lett.,* **40,** 4048–4053, doi:10.1002/grl.50685.

Capotondi, A., and A. Wittenberg, 2013: ENSO diversity in climate models. *U.S. CLIVAR Variations,* No. 2, U.S. CLIVAR, Washington, DC, 10–14.

Choi, J., S.-I. An, J.-S. Kug, and S.-W. Yeh, 2011: The role of mean state on changes in El Niño's flavor. *Climate Dyn.,* **37,** 1205–1215, doi:10.1007/s00382-010-0912-1.

——, ——, and S.-W. Yeh, 2012: Decadal amplitude modulation of two types of ENSO and its relationship with the mean state. *Climate Dyn.,* **38,** 2631–2644, doi:10.1007/s00382-011-1186-y.

Chou, C., J. C. H. Chaing, C.-W. Lan, C.-H. Chung, Y.-C. Liao, and C.-J. Lee, 2013: Increase in the range between wet and dry season precipitation. *Nat. Geosci.,* **6,** 263–267, doi:10.1038/ngeo1744.

Clarke, A. J., 1994: Why are surface equatorial ENSO winds anomalously westerly under anomalous large-scale convection? *J. Climate,* **7,** 1623–1627, doi:10.1175/1520-0442(1994)007<1623:WASEEW>2.0.CO;2.

Dai, A., 2006: Precipitation characteristics in eighteen coupled climate models. *J. Climate,* **19,** 4605–4630, doi:10.1175/JCLI3884.1.

Fedorov, A. V., and S. G. Philander, 2001: A stability analysis of tropical ocean–atmosphere interactions: Bridging measurements and theory for El Nino. *J. Climate,* **14,** 3086–3101, doi:10.1175/1520-0442(2001)014<3086:ASAOTO>2.0.CO;2.

Fennessy, M. J., and Coauthors, 1994: The simulated Indian monsoon: A GCM sensitivity study. *J. Climate,* **7,** 33–43, doi:10.1175/1520-0442(1994)007<0033:TSIMAG>2.0.CO;2.

Gent, P. R., and Coauthors, 2011: The Community Climate System Model version 4. *J. Climate,* **24,** 4973–4991, doi:10.1175/2011JCLI4083.1.

Guilyardi, E., and Coauthors, 2009: Understanding El Niño in ocean–atmosphere general circulation models: Progress and challenges. *Bull. Amer. Meteor. Soc.,* **90,** 325–340, doi:10.1175/2008BAMS2387.1.

Ham, Y.-G., and J.-S. Kug, 2012: How well do current climate models simulate two types of El Niño? *Climate Dyn.,* **39,** 383–398, doi:10.1007/s00382-011-1157-3.

——, and ——, 2014: ENSO phase-locking to the boreal winter in CMIP3 and CMIP5 models. *Climate Dyn.,* **43,** 305–318, doi:10.1007/s00382-014-2064-1.

——, ——, I.-S. Kang, F.-F. Jin, and A. Timmermann, 2010: Impact of diurnal atmosphere–ocean coupling on tropical climate simulations using a coupled GCM. *Climate Dyn.,* **34,** 905–917, doi:10.1007/s00382-009-0586-8.

——, I.-S. Kang, D. Kim, and J.-S. Kug, 2012: El Niño–Southern Oscillation simulated and predicted in SNU coupled GCMs. *Climate Dyn.,* **38,** 2227–2242, doi:10.1007/s00382-011-1171-5.

——, M. Lim, and J.-S. Kug, 2013: Importance of mean state in simulating different types of El Niño revealed by SNU coupled GCMs. *Prog. Oceanogr.,* **116,** 130–141, doi:10.1016/j.pocean.2013.07.005.

——, S. Schubert, Y. Vikhliaev, and M. J. Suarez, 2014: An assessment of the skill of GEOS-5 seasonal forecasts. *Climate Dyn.,* **43,** 2415–2430, doi:10.1007/s00382-014-2063-2.

Harrison, D. E., and G. A. Vecchi, 1999: On the termination of El Niño. *Geophys. Res. Lett.,* **26,** 1593–1596, doi:10.1029/1999GL900316.

Held, I. M., and B. J. Soden, 2006: Robust responses of the hydrological cycle to global warming. *J. Climate,* **19,** 5686–5699, doi:10.1175/JCLI3990.1.

Jang, Y.-S., D. Kim, Y.-H. Kim, D.-H. Kim, M. Watanabe, F.-F. Jin, and J.-S. Kug, 2013: Simulation of two types of El Niño from different convective parameters. *Asia-Pac. J. Atmos. Sci.,* **49,** 193–199, doi:10.1007/s13143-013-0020-3.

Kang, I.-S., and Coauthors, 2002: Intercomparison of the climatological variations of Asian summer monsoon precipitation simulated by 10 GCMs. *Climate Dyn.,* **19,** 383–395, doi:10.1007/s00382-002-0245-9.

Kao, H.-Y., and J.-Y. Yu, 2009: Contrasting eastern-Pacific and central-Pacific types of ENSO. *J. Climate,* **22,** 615–632, doi:10.1175/2008JCLI2309.1.

Kim, D., J.-S. Kug, I.-S. Kang, F.-F. Jin, and A. Wittenberg, 2008: Tropical Pacific impacts of convective momentum transport in the SNU coupled GCM. *Climate Dyn.,* **31,** 213–226, doi:10.1007/s00382-007-0348-4.

——, Y.-S. Jang, D.-H. Kim, Y.-H. Kim, M. Watanabe, F.-F. Jin, and J. S. Kug, 2011a: El Niño–Southern Oscillation sensitivity to cumulus entrainment in a coupled general circulation model. *J. Geophys. Res.,* **116,** D22112, doi:10.1029/2011JD016526.

——, A. H. Sobel, E. D. Maloney, D. M. W. Frierson, and I.-S. Kang, 2011b: A systematic relationship between intraseasonal variability and mean state bias in AGCM simulations. *J. Climate,* **24,** 5506–5520, doi:10.1175/2011JCLI4177.1.

Kim, S.-T., and J.-Y. Yu, 2012: The two types of ENSO in CMIP5 models. *Geophys. Res. Lett.,* **39,** L11704, doi:10.1029/2012GL052006.

——, W. Cai, F.-F. Jin, and J.-Y. Yu, 2013: ENSO stability in coupled climate models and its association with mean state. *Climate Dyn.,* **42,** 3313–3321, doi:10.1007/s00382-013-1833-6.

Kirtman, B. P., Y. Fan, and E. K. Schneider, 2002: The COLA global coupled and anomaly coupled ocean–atmosphere GCM. *J. Climate,* **15,** 2301–2320, doi:10.1175/1520-0442(2002)015<2301:TCGCAA>2.0.CO;2.

——, and Coauthors, 2014: The North American Multimodel Ensemble (NMME): Phase-1 seasonal to interannual prediction; phase-2 toward developing intra-seasonal prediction. *Bull. Amer. Meteor. Soc.,* **95,** 585–601, doi:10.1175/BAMS-D-12-00050.1.

Knutson, T. R., and S. Manabe, 1995: Time-mean response over the tropical Pacific to increased CO_2 in a coupled ocean–atmosphere model. *J. Climate,* **8,** 2181–2199, doi:10.1175/1520-0442(1995)008<2181:TMROTT>2.0.CO;2.

Kug, J.-S., and I.-S. Kang, 2006: Interactive feedback between ENSO and the Indian Ocean. *J. Climate,* **19,** 1784–1801, doi:10.1175/JCLI3660.1.

——, B. P. Kirtman, and I.-S. Kang, 2006: Interactive feedback between ENSO and the Indian Ocean in an interactive coupled model. *J. Climate,* **19,** 6371–6381, doi:10.1175/JCLI3980.1.

——, I.-S. Kang, and D.-H. Choi, 2008: Seasonal climate predictability with tier-one and tier-two prediction systems. *Climate Dyn.,* **31,** 403–416, doi:10.1007/s00382-007-0264-7.

——, F.-F. Jin, and S.-I. An, 2009: Two types of El Niño events: Cold tongue El Niño and warm pool El Niño. *J. Climate,* **22,** 1499–1515, doi:10.1175/2008JCLI2624.1.

——, J. Choi, S.-I. An, F.-F. Jin, and A. Wittenberg, 2010: Warm pool and cold tongue El Niño events as simulated by the GFDL2.1 coupled GCM. *J. Climate,* **23,** 1226–1239, doi:10.1175/2009JCLI3293.1.

——, Y.-G. Ham, J.-Y. Lee, and F.-F. Jin, 2012: Improved simulation of two types of El Niño in CMIP5 models. *Environ. Res. Lett.,* **7,** 034002, doi:10.1088/1748-9326/7/3/034002.

Lau, N.-C., and M. J. Nath, 2000: Impact of ENSO on the variability of the Asian–Australian monsoon as simulated in GCM experiments. *J. Climate,* **13,** 4287–4309, doi:10.1175/1520-0442(2000)013<4287:IOEOTV>2.0.CO;2.

Lee, J.-Y., and Coauthors, 2010: How are seasonal prediction skills related to models' performance on mean state and annual cycle? *Climate Dyn.,* **35,** 267–283, doi:10.1007/s00382-010-0857-4.

Lin, J.-L., 2007: The double-ITCZ problem in IPCC AR4 coupled GCMs: Ocean–atmosphere feedback analysis. *J. Climate,* **20,** 4497–4525, doi:10.1175/JCLI4272.1.

Misra, V., and Coauthors, 2007: Validating and understanding the ENSO simulation in two coupled climate models. *Tellus,* **59A,** 292–308, doi:10.1111/j.1600-0870.2007.00231.x.

Neale, R. B., J. H. Richter, and M. Jochum, 2008: The impact of convection on ENSO: From a delayed oscillator to a series of events. *J. Climate,* **21,** 5904–5924, doi:10.1175/2008JCLI2244.1.

O'Gorman, P., 2012: Sensitivity of tropical precipitation extremes to climate change. *Nat. Geosci.,* **5,** 697–700, doi:10.1038/ngeo1568.

Santoso, A., S. McGregor, F.-F. Jin, W. Cai, M. H. England, S.-I. An, M. J. McPhaden, and E. Guilyardi, 2013: Late-twentieth-century emergence of the El Niño propagation asymmetry and future projections. *Nature,* **504,** 126–130, doi:10.1038/nature12683.

Spencer, H., and J. M. Slingo, 2003: The simulation of peak and delayed ENSO teleconnections. *J. Climate,* **16,** 1757–1774, doi:10.1175/1520-0442(2003)016<1757:TSOPAD>2.0.CO;2.

Sperber, K. R., and T. N. Palmer, 1996: Interannual tropical rainfall variability in general circulation model simulations associated with the Atmospheric Model Intercomparison Project. *J. Climate,* **9,** 2727–2750, doi:10.1175/1520-0442(1996)009<2727:ITRVIG>2.0.CO;2.

Taylor, K. E., R. J. Stouffer, and G. A. Meehl, 2012: An overview of CMIP5 and the experiment design. *Bull. Amer. Meteor. Soc.,* **93,** 485–498, doi:10.1175/BAMS-D-11-00094.1.

Turner, A. G., P. M. Inness, and J. M. Slingo, 2005: The role of the basic state in the ENSO–monsoon relationship and implications for predictability. *Quart. J. Roy. Meteor. Soc.,* **131,** 781–804, doi:10.1256/qj.04.70.

Wang, B., and S.-I. An, 2001: Why the properties of El Niño changed during the late 1970s. *Geophys. Res. Lett.,* **28,** 3709–3712, doi:10.1029/2001GL012862.

Watanabe, M., and Coauthors, 2010: Improved climate simulation by MIROC5: Mean states, variability, and climate sensitivity. *J. Climate,* **23,** 6312–6335, doi:10.1175/2010JCLI3679.1.

——, M. Chikira, Y. Imada, and M. Kimoto, 2011: Convective control of ENSO simulated in MIROC. *J. Climate,* **24,** 543–562, doi:10.1175/2010JCLI3878.1.

Wentz, F. J., L. Ricciardulli, K. Hilburn, and C. Mears, 2007: How much more rain will global warming bring? *Science,* **317,** 233–235, doi:10.1126/science.1140746.

Wittenberg, A. T., A. Rosati, N.-C. Lau, and J. J. Ploshay, 2006: GFDL's CM2 global coupled climate models. Part III: Tropical Pacific climate and ENSO. *J. Climate,* **19,** 698–722, doi:10.1175/JCLI3631.1.

Yeh, S.-W., J.-S. Kug, B. Dewitte, M.-H. Kwon, B. Kirtman, and F.-F. Jin, 2009: El Niño in a changing climate. *Nature,* **461,** 511–514, doi:10.1038/nature08316.

——, Y.-G. Ham, and J.-Y. Lee, 2012: Changes in the tropical Pacific SST trend from CMIP3 to CMIP5 and its implication of ENSO. *J. Climate,* **25,** 7764–7771, doi:10.1175/JCLI-D-12-00304.1.

——, ——, and B. P. Kirtman, 2014a: A possible explanation on the changes in the spatial structure of ENSO from CMIP3 to CMIP5. *Geophys. Res. Lett.,* **41,** 140–145, doi:10.1002/2013GL058478.

——, J.-S. Kug, and S.-I. An, 2014b: Recent progress on two types of El Niño: Observations, dynamics, and future changes. *Asia-Pac. J. Atmos. Sci.,* **50,** 69–81, doi:10.1007/s13143-014-0028-3.

Yu, J. Y., and S. T. Kim, 2010: Three evolution patterns of central-Pacific El Niño. *Geophys. Res. Lett.,* **37,** L08706, doi:10.1029/2010GL042810.

Zhang, T., and D.-Z. Sun, 2014: ENSO asymmetry in CMIP5 models. *J. Climate,* **27,** 4070–4093, doi:10.1175/JCLI-D-13-00454.1.

Zhang, W., and F.-F. Jin, 2012: Improvements in the CMIP5 simulations of ENSO-SSTA meridional width. *Geophys. Res. Lett.,* **39,** L23704, doi:10.1029/2012GL053588.